A Systematic Approach to Predicting Critical Heat Flux for Inclined Sprays

Milan Visaria

Issam Mudawar[1]
e-mail: mudawar@ecn.purdue.edu

Purdue University International Electronic Cooling Alliance (PUIECA),
585 Purdue Mall,
West Lafayette, IN 47907

This study provides a new systematic approach to predicting the effects of spray inclination on critical heat flux (CHF). Experiments were performed with three pressure spray nozzles over a broad range of inclination angles at five flow rates and subcoolings of 15°C *and* 25°C. *These experiments also included high-speed video analysis of spray formation, impact, and recoil for a* 1.0×1.0 cm^2 *test surface. Inclined sprays produced elliptical impact areas, distorted by lateral liquid flow that provided partial resistance to dryout along the downstream edge of the impact ellipse. These observations are used to determine the locations of CHF commencement along the test surface. A new theoretical model shows that increasing inclination angle away from normal decreases both the spray impact area and the volumetric flux. These trends explain the observed trend of decreasing CHF with increasing inclination angle. Combining the new model with a previous point-based CHF correlation shows great success in predicting the effects of spray inclination on CHF.* [DOI: 10.1115/1.2804095]

Introduction

For many decades, spray cooling has been used in a variety of applications demanding rapid cooling of metal parts from elevated temperatures [1–5]. One such application is quenching, where the temperature of an alloy is dropped quickly from slightly below the melting point to room temperature to preserve microstructure during heat treatment. In fact, much of the spray cooling literature concerns high surface temperatures corresponding mostly to the film boiling regime, and efforts have been focused on expediting the onset of the Leidenfrost point to take advantage of the higher heat transfer coefficients (i.e., achieve faster cooling) during the ensuing transition boiling regime [6]. Two types of sprays have been utilized in these applications, pressure sprays and air-assist sprays. Pressure sprays utilize high-pressure drop across the spray nozzle, as well as swirl features inside the nozzle itself, to overcome surface tension forces, breaking the liquid to a large number of droplets. Air-assist sprays, on the other hand, rely on a secondary high-pressure air stream that is supplied in a swirl pattern to achieve the breakup. The goal with both types of sprays is to ensure liquid breakup into small droplets having high surface-area-to-volume ratio, as well as to increase the momentum of droplet impact with the hot surface.

The past two decades have witnessed significant interest in the implementation of spray cooling for heat removal from high performance electronic devices [7–11]. This application is categorically different from quenching in terms of both surface temperature range and spray type. Unlike metal alloy parts, the temperature of an electronic device must be kept safely below a limit dictated by the device materials and reliability. This implies that spray cooling must maintain device temperatures within the single-phase and nucleate boiling regimes, safely below the critical heat flux (CHF) limit. Furthermore, air-assist sprays are undesirable in electronic cooling because of the difficulty in separating air from the primary coolant, let alone the drastically negative impact of air on condenser performance in a closed two-phase loop.

Spray cooling of electronics is an aggressive cooling scheme involving high momentum droplet impact with the device surface. As such, it is a direct competitor to jet-impingement cooling. A spray is often preferred to a single jet impinging the center of a device because of the spray's ability to provide better surface temperature uniformity. However, the sharp concentration of cooling in the impingement zone of a jet can be lessened with slot jets or multiple circular jets. The relative merits of a spray versus a slot jet or multiple circular jets remain elusive. However, the reluctance to use sprays for electronics cooling has less to do with temperature uniformity than with practical nozzle-related concerns. A comprehensive assessment of common spray nozzles by Hall and Mudawar [4,5] showed that seemingly identical commercial nozzles sometimes produce drastically different spray patterns because of minute manufacturing imperfections of the intricate swirl passages inside the nozzle itself. They also demonstrated experimentally that the same spray nozzle might display appreciable changes in cooling behavior over time because of corrosion and/or erosion effects. They recommended several practical guidelines to help alleviate these problems. Nonetheless, those same problems will become far more serious with a new class of microspray nozzles that are being proposed for electronics cooling.

Another drawback of sprays is the minimum orifice-to-surface distance required to ensure a fully developed spray pattern. This distance allows for initial breakup of the liquid into liquid sheets, followed by tubular ligaments, and ultimately individual droplets [12]. Stringent packaging constraints of electronic assemblies often preclude the space required to ensure spray breakup. Two techniques that are used to cope with the space constraints are tilting the spray from normal orientation relative to the device surface and using microsprays that require shorter breakup distances.

However, perhaps the most difficult aspect of implementing spray cooling is poor understanding of many of the underlying mechanisms of droplet breakup, impact, and boiling. Understanding these mechanisms is complicated by the large number of parameters that influence spray behavior, such as droplet size, droplet velocity, droplet number density, nozzle type and size, spray angle, orifice-to-surface distance, and inclination angle [7,8]. Despite much dedicated research effort, the large number of spray parameters has made it quite difficult to ensure adequate coverage of relevant parametric ranges. This is especially the case with the effects of geometrical parameters on nucleate boiling and CHF.

[1]Corresponding author.

Contributed by the Electrical and Electronic Packaging Division of ASME for publication of the JOURNAL OF ELECTRONIC PACKAGING. Manuscript received October 16, 2006; final manuscript received March 26, 2007. Review conducted by Andrew Y.-H. Hung.

Failure to adhere to strict geometrical constraints can greatly compromise the usefulness of any spray cooling study. Situating the nozzle in close proximity to the device surface tends to concentrate all the droplet impact in a small central portion of the device surface. On the other hand, moving the nozzle far from the device surface causes a significant fraction of the droplets to fall wastefully outside the device surface. Estes and Mudawar [7,8] developed a theoretical model to aid in optimizing the orifice-to-surface distance for a pressure spray impacting a square heated surface. Optimum (highest) CHF was measured when the orifice-to-surface distance was such that the spray impact area just inscribes the device surface, and orifice-to-surface distances that were either smaller or larger than optimum yielded smaller CHF.

Another important geometrical parameter for spray cooling is the angle of inclination α from the normal to the device surface. Intuitively, one might assume that CHF is highest when the spray is normal to the surface ($\alpha=0$ deg). This orientation ensures that droplets utilize their full near-vertical momentum upon impact. However, as mentioned earlier, electronics applications sometimes preclude the use of a normal spray orientation because of packaging constraints. In such applications, it is necessary to tilt the spray relative to the normal. A key challenge in those situations is to determine the effect of spray inclination on CHF. This is a key objective of the present study.

Very few published studies address the effects of spray inclination on two-phase cooling performance. Silk et al. [13] sprayed flat and enhanced copper surfaces with PF-5060 at spray inclinations of $\alpha=0$ deg, 30 deg, and 45 deg with the normal to the surface while maintaining a constant orifice-to-surface distance. For both types of surfaces, CHF was maximum for $\alpha=30$ deg, a phenomenon they attributed to the sweeping motion of the spray droplet's horizontal velocity component while maintaining a dominant vertical velocity component. In a study by Li et al. [14], spray inclination angle was increased from 0 deg to 60 deg in 20 deg increments while maintaining a constant orifice-to-surface distance. CHF increased when α was increased from 0 deg to 40 deg and decreased sharply above 40 deg. The sharp decrease was attributed to an appreciable fraction of liquid missing the test surface and to low spray momentum flux at large inclination angles. The studies by Silk et al. and Li et al. point to the great importance of understanding the effects of spray inclination on electronics cooling.

The present study will explore the variation of CHF with spray inclination for different nozzles, flow rates, and subcoolings. Building on a recent study by the authors [15], spray inclination was varied from 0 deg (spray axis normal to surface) to 55 deg. Unlike the studies by Silk et al. and Li et al., where the orifice-to-surface distance was kept constant, this distance was changed in the present study for each nozzle and inclination angle such that the spray impact area just inscribes a square test surface. This ensured that CHF is maximum for each configuration [8]. A recent model by the authors [15], which predicts volumetric flux distribution for different spray inclinations, is combined with a previous point-based CHF correlation by Estes and Mudawar [7] to recommend a new systematic method in predicting CHF for inclined sprays.

Experimental Methods

Spray experiments were performed inside a rectangular test chamber using PF-5052 as working fluid. Relevant properties of saturated PF-5052 at 1 atm ($T_{sat}=50°C$) are as follows: $\rho_f=1643$ kg/m^3, $\rho_g=12.0$ kg/m^3, $\sigma=0.013$ N/m, $h_{fg}=104,700$ J/kg, $c_{p,f}=1092$ J/kg K, $\mu_f=517\times10^{-6}$ N s/m^2, and $k_f=0.058$ W/m K. The chamber was fabricated mostly from G-10 fiberglass plastic and fitted with front and side windows made from transparent polycarbonate plastic. The test heater was mounted a short distance above the base of the test chamber. The nozzle inclination angle and orifice-to-surface distance were adjusted with the aid of a nozzle positioning system illustrated in Fig. 1. This system featured vertical, horizontal, and angular positioning stages. Vertical translation was achieved with an aluminum block that was mounted on two aluminum rods that ran vertically through the test chamber. A micrometer translation stage was attached externally to guide vertical translation of the nozzle assembly. A horizontal stage was slid through a rectangular groove in the vertical stage. The nozzle assembly was positioned manually in the horizontal direction, guided by a small scale. Mounted to the horizontal stage was a third rotation stage that was notched with a series of holes spanning 0–90 deg angles in 5 deg increments. The spray nozzle was held on a bracket that was attached to the rotation stage at both the center of rotation and one of the holes. The nozzle inclination angle was set by positioning a pin through the nozzle bracket and into the desired hole.

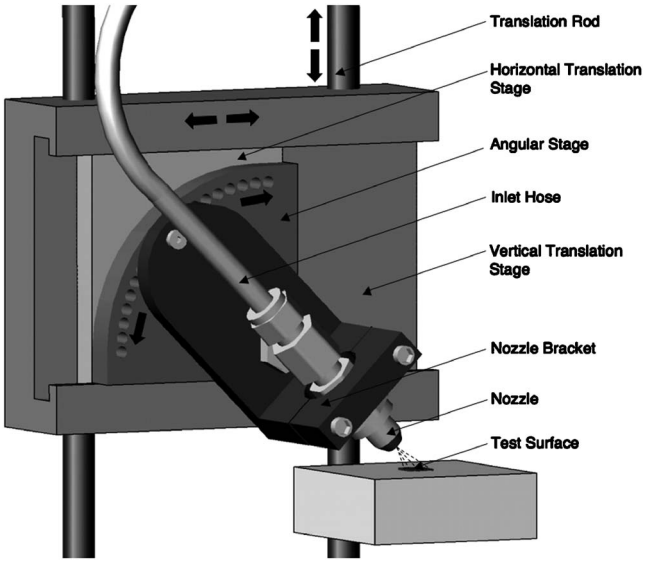

Fig. 1 Nozzle positioning system inside the spray chamber

The 1.0×1.0 cm^2 test surface formed the end of the extended square neck of a large oxygen-free copper block. The enlarged underside of the copper block was bored to accept nine 220 W cartridge heaters that supplied heat to the test surface. The test surface was insulated with high-temperature G-7 fiberglass plastic to both reduce heat loss and ensure 1D conduction through the neck leading to the test surface. Embedded 1.27 mm beneath the test surface, a type-K (Chromel-Alumel) thermocouple was used to measure the surface temperature. Further details of the construction of the test heater can be found elsewhere [16].

Fluid supply and conditioning were achieved with a two-phase flow loop illustrated schematically in Fig. 2. After impinging the test surface, some of the coolant was converted to vapor that rose to the top region of the test chamber while unevaporated liquid drained through the bottom of the test chamber. Both the vapor and liquid were routed to the loop's reservoir. The liquid proceeded to drain to a deaeration chamber situated beneath the reservoir while the vapor was condensed to liquid inside an air-cooled condenser then dripped back to the reservoir. Two magnetically coupled centrifugal pumps were connected in parallel to provide the required flow rate. The pumped liquid flowed through a filter followed by one of two rotameters connected in parallel. The fluid then entered a finned-tube heat exchanger that was cooled by two high-capacity fans. This heat exchanger served as a precooler to achieve the required subcooling as the coolant entered the test chamber.

The experiments were performed using three Unijet full-cone nozzles made by Spraying Systems Company. Table 1 shows the key hydrodynamic properties of the sprays. Before initiating an experiment, calculations were made to determine the horizontal

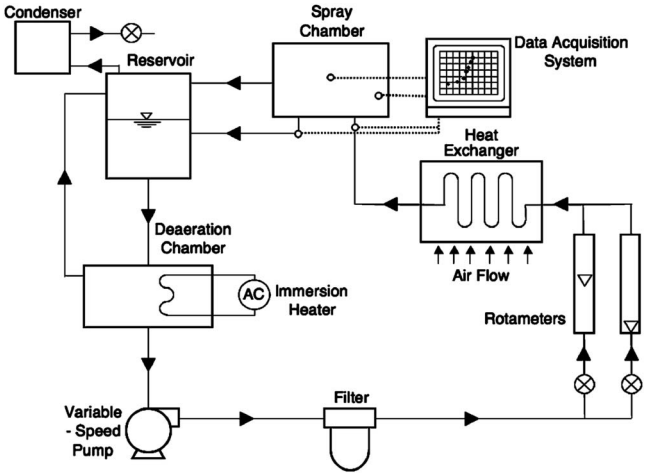

Fig. 2 Two-phase spray cooling loop

and vertical positions of the nozzle from the test surface such that the spray impact area just inscribes the heater surface. The test chamber was then sealed and the reservoir charged with coolant. The coolant was carefully deaerated throughout the flow loop to expel any noncondensable gases to the ambient. This was achieved by first boiling the fluid vigorously for about 30 min in the deaeration chamber with the aid of an immersion heater. Mixed with noncondensable gases, the vapor produced flowed to the upper region of the reservoir followed by the condenser above. The vapor condensed and was recovered while any noncondensable gases were expelled to the ambient through a vent. The pump was then turned on to circulate the coolant through the loop, and the deaeration process continued for about an additional 15 min. The condenser vent was then closed to seal the loop from the ambient. The pump controllers were adjusted to the desired flow rate and the precooler fans turned on to achieve the desired coolant temperature at the nozzle inlet. Atmospheric pressure was maintained inside the chamber at all times.

Once the required operating conditions were achieved, electrical power was supplied to the cartridge heaters by a variable voltage transformer. The power input was measured with a 0.5% accuracy Yokogawa digital wattmeter. Thermal analysis showed that less than 2% of the power input was lost to the ambient [16]. Thus, the total errors in heat flux measurement were +0.5% and −2.51%. Boiling curves were generated by increasing voltage supply to the heaters in small increments. Boiling data were recorded following each increment after the test heater reached steady state. Small voltage increments ensured accurate CHF detection and measurement. CHF was detected by an unsteady increase in the heater surface temperature, prompting the operator to manually cut off the electrical power input to the heater.

Pressure and temperature sensors were placed inside the test chamber as well as the test chamber's inlet and outlets. Uncertainties in the pressure, flow rate, and temperature measurements were less than 0.5%, 1.0%, and ±0.2 °C, respectively.

Table 1 Characteristics of spray nozzles utilized in the present study

Nozzle	Orifice diameter d_o (mm)	Spray angle θ (deg)	Sauter mean diameter d_{32} (10^6 m)	Volumetric flow rate Q (10^6 m^3 s^{-1})
1	0.762	55.8	111–123	3.50–3.86
2	1.19	46.4	160–179	4.97–13.4
3	1.70	48.5	189–249	17.02

Flow Visualization

High-speed video motion analysis played a vital role in capturing droplet breakup and impact, as well as the ensuing liquid flow for different inclination angles. Video segments were recorded using a FASTCAM-Ultima APX FM camera capable of recording speeds of 2000 frames/s at full resolution (1024 × 1024) and up to 120,000 frames/s at reduced resolution. Optimum spray image quality was achieved at 6000 frames/s with a resolution of 512 × 512 using a shutter speed of 1/6000 s.

Figure 3 shows still images of the spray that were extracted from the high-speed video records of spray Nozzle 1 for a relatively high flow rate of 3×10^{-6} m^3/s, which is within the recommended operating range for this nozzle. Shown side by side are representative images for adiabatic conditions (zero heat flux) and at 90–95% of CHF. Several important features are readily apparent from these images. Recall that the orifice-to-surface distance was adjusted for each inclination angle such that the spray just inscribes the test surface (i.e., major axis of spray impact ellipse is equal to width of test surface). Figure 3 shows adherence to this criterion while increasing inclination angle brings the spray nozzle closer to the test surface. The orifice-to-surface distance is largest for normal impact, α=0 deg, and smallest for α=55 deg. Increasing the inclination angle beyond 55 deg was not possible as this would require the edge of the spray nozzle to fall below the plane of the test surface.

Figure 3 shows near-perfect symmetry in droplet distribution with respect the spray axis for α=0 deg. The spray impact area for this normal orientation is a circle whose diameter is equal to the width of the test surface. For adiabatic impact, the spray droplets impinge the test surface, spread, and break up into smaller droplets that are ejected at different angles relative to the test surface. At pre-CHF conditions, intense evaporation and boiling causes violent breakup and recoil of the impinging droplets (a more detailed discussion on this topic is given in Ref. [17]). Relatively large droplets are shown recoiling at an angle to the test surface. Increasing the inclination even by a small angle of 10 deg caused appreciable lateral flow of liquid parallel to the test surface. The liquid flow consists of both a thin liquid film flowing along the surface and ejected droplets moving in close vicinity to the surface. The pre-CHF condition shows larger droplets bouncing off the surface. The lateral liquid flow becomes more appreciable at high inclination angles.

Figure 4 shows both adiabatic and pre-CHF images of Nozzle 1 sprays at a relatively low flow rate of 4.5×10^{-7} m^3/s. This flow rate was purposely selected below the normal operating range for this nozzle to investigate the effects of low flow rate on spray behavior. Like the higher flow rate sprays depicted in Fig. 3, increasing inclination angle causes lateral liquid flow along the surface. However, given the small spray flow rate, a large fraction of the impinging liquid is evaporated compared to the sprays depicted in Fig. 3. Figure 4 shows incomplete breakup of the spray liquid caused by the very low flow rate tested. The breakup is further compromised at large inclination angles because of the short distance available for droplet breakup at these orientations. By comparison, Fig. 3 shows fully developed breakup for all inclination angles at the higher flow rate.

One of the key objectives of the high-speed video analysis is to explore the influences of the spray's geometrical parameters on CHF. A previous study by Estes and Mudawar [8] showed that CHF for normal sprays is influenced by two spray parameters, Sauter mean diameter d_{32} and volumetric flux. While d_{32} is fairly constant everywhere in a fully developed spray, volumetric flux varies with both orifice-to-surface distance and distance from the nozzle axis. For a normal spray, volumetric flux is smallest along the outer perimeter of the impact circle; CHF therefore commences at the perimeter and its magnitude should be based on the value of volumetric flux along the perimeter. The center of the impact circle for a normal spray (α=0 deg) coincides with the center of the test surface. However, as the inclination angle in-

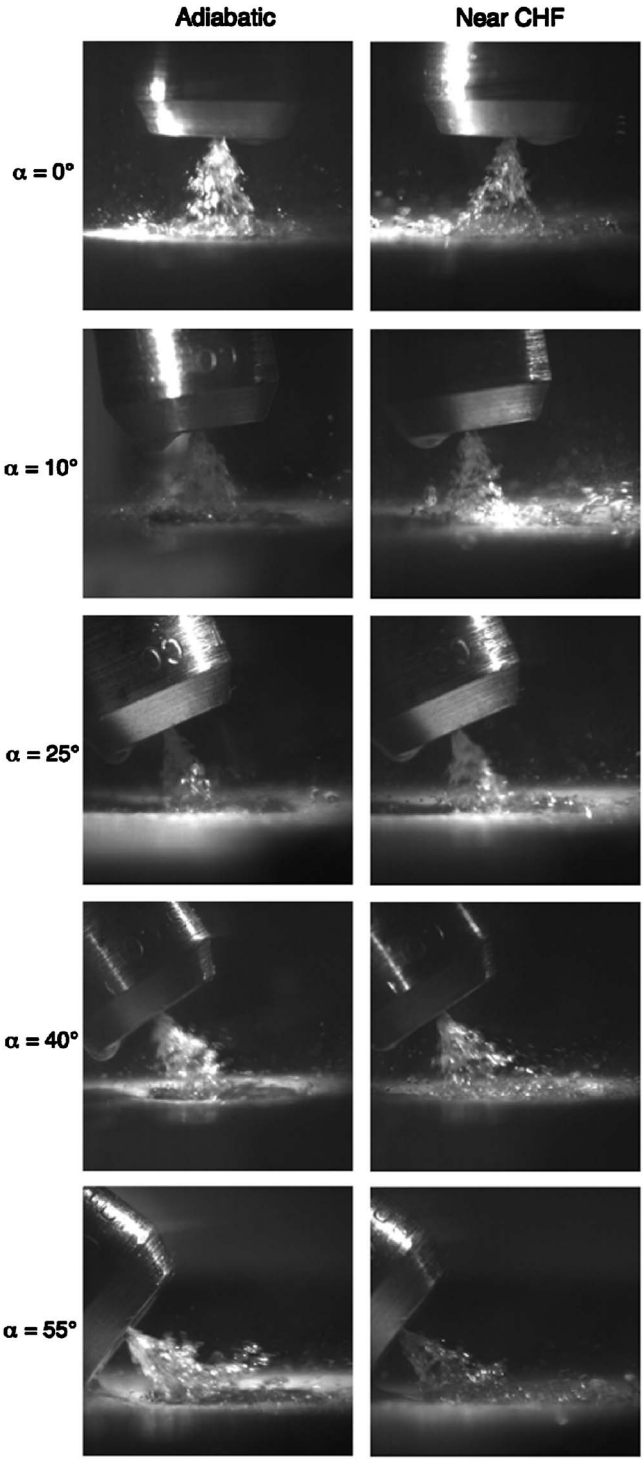

Fig. 3 Images of Nozzle 1 sprays at relatively high flow rate of 3×10^{-6} m^3/s for adiabatic and pre-CHF conditions

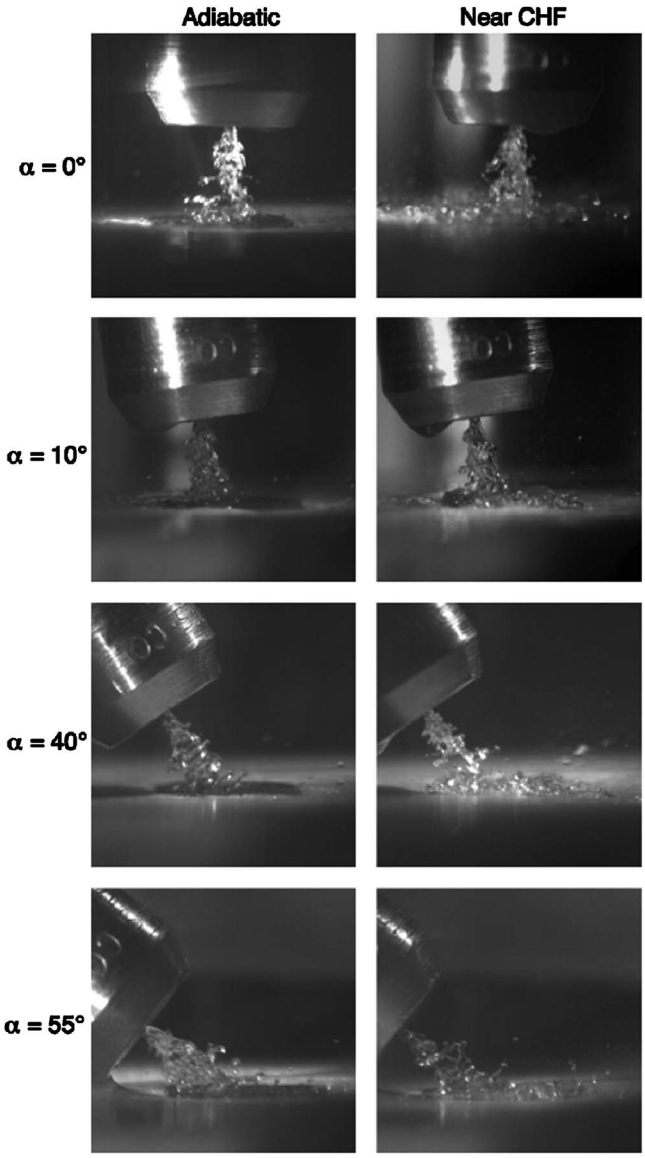

Fig. 4 Images of Nozzle 1 sprays at relatively low flow rate of 4.5×10^{-7} m^3/s for adiabatic and pre-CHF conditions

creases, the impact area becomes an ellipse whose center is shifted away from the center and toward the upstream edge of the test surface. This behavior is clearly manifested in Figs. 3 and 4. This shift is the result of the aforementioned constraint requiring the impact area to just inscribe the test surface. For $\alpha>0$ deg, this implies that the major axis of the spray equals the width of the test surface. Based on geometrical considerations alone, the volumetric flux for an inclined spray should be lowest at the outermost point of the major axis. This is the location farthest from the nozzle orifice. Intuitively, one might conclude that CHF for an inclined spray commences at this location.

However, Figs. 3 and 4 show that tilting the spray away from normal causes lateral liquid flow along the heater surface in addition to the direct impingement of spray droplets. The lateral flow is believed to resist dryout at the aforementioned location of the weakest volumetric flux. It can therefore be concluded that CHF will occur at points along the perimeter of the impact ellipse that (1) are farthest from the spray orifice and (2) do not benefit from the lateral liquid flow. Figure 5 shows that these conditions correspond to the two end points of the minor axis of the impact ellipse. CHF prediction therefore requires accurate determination of volumetric flux at these end points.

CHF Results

Boiling curves were measured at 1 atm for three spray nozzles using PF-5052 as working fluid at flow rates of 3.5×10^{-6} m^3/s to 1.7×10^{-5} m^3/s and subcoolings of 15°C and 25°C. Experiments were repeated for inclination angles of $\alpha=0$ deg, 10 deg, 25 deg, 40 deg, and 55 deg. Visaria and

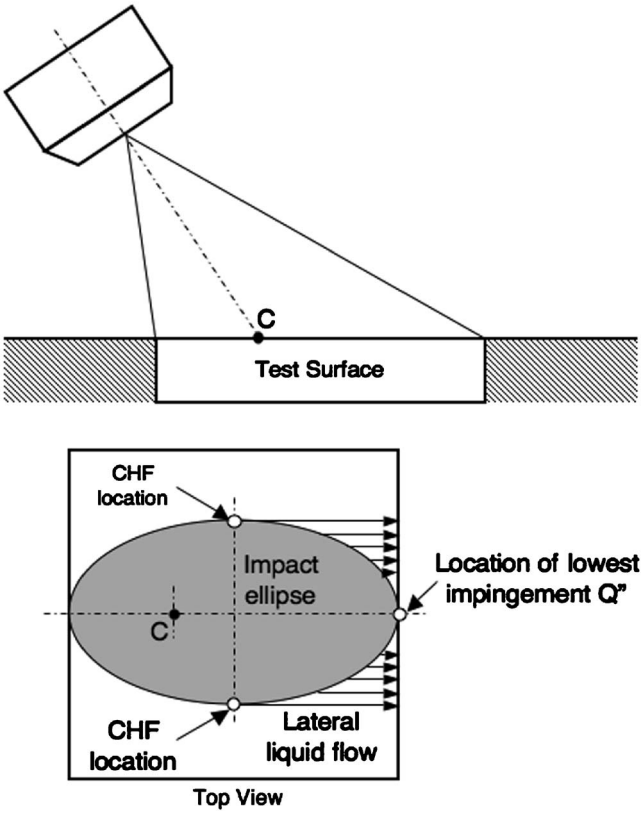

Fig. 5 Locations of CHF commencement

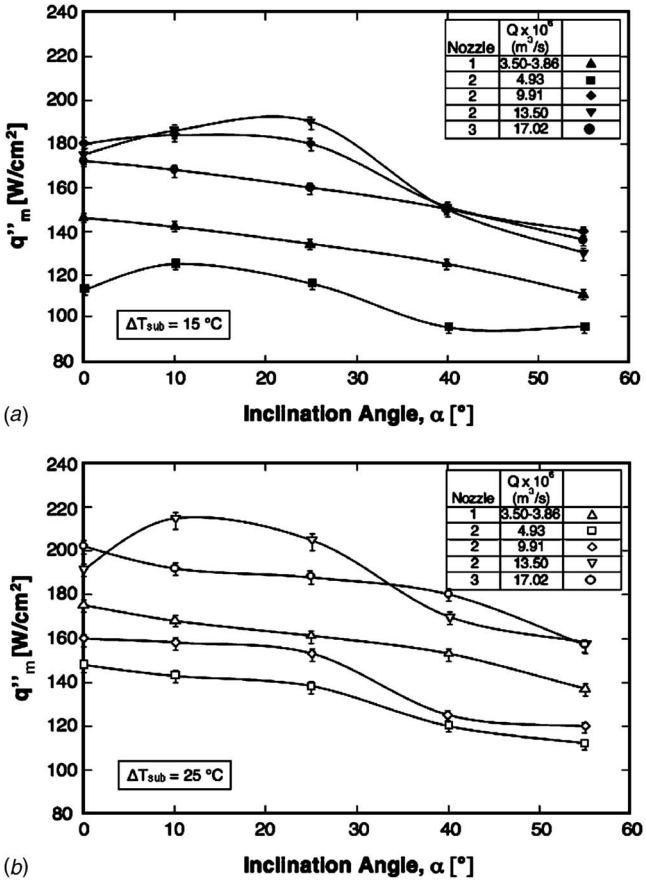

Fig. 6 Variation of CHF with inclination angle for three nozzles at (a) $\Delta T_{sub}=15^{\circ}C$ and (b) $\Delta T_{sub}=25^{\circ}C$

Mudawar [15] showed that inclination angle does not have a pronounced effect on the single-phase or nucleate boiling regions. However, their boiling curves showed substantial variation in CHF with α. Increased subcooling and/or spray flow rate delayed both the onset of subcooling and CHF.

Figures 6(*a*) and 6(*b*) show CHF variations with inclination angle for different flow rates corresponding to subcoolings of 15°C and 25°C, respectively. CHF in these two figures is the measured electrical power input divided by the total area (L^2) of the test surface. Both figures show a general trend of decreasing CHF with increasing α. With a few exceptions, CHF was greatest for each nozzle for normal impact ($\alpha=0$ deg) and lowest for the largest inclination angle tested, 55 deg. Figures 6(*a*) and 6(*b*) show a fairly monotonic trend of increasing CHF for a given nozzle and inclination angle with increasing flow rate and increasing subcooling. There are a few exceptions. Some of the Nozzle 2 flow rates appear to produce a CHF maximum closer to $\alpha=10$ deg rather than to $\alpha=0$ deg. However, CHF difference between the two locations is too small to constitute a systematic trend for this particular nozzle.

Geometrical Considerations

In a recent article by the authors of the present study [15], an earlier model of volumetric flux distribution for a normal spray by Estes and Mudawar [7,8] was extended to inclined sprays. Like the original model, the spray orifice was assumed to represent a uniform point source for the sprayed fluid. This implied volumetric flux is constant across any spherical surface centered at the nozzle orifice and bounded by the spray cone angle θ. However, volumetric flux varies across any surface perpendicular to the spray axis (as in normal sprays) and these variations increase with increasing inclination angle. This behavior is illustrated in Fig. 7. Here, volumetric flux is constant everywhere along spherical area A' located a distance H from the orifice but is projected nonuniformly on imaginary surface A'' perpendicular to the spray axis. The volumetric flux decreases radially outward along A'' away from the spray axis. Figure 7 shows the projection of the spray liquid onto test surface A for an inclined spray. The volumetric flux for an infinitesimal area dA of the test surface is smaller than for dA' of the spherical surface because of the farther location of dA from the orifice compared to dA'. Volumetric flux shows appreciable variation along surface A because of the large variations in distance from the orifice along this surface. Increasing inclination angle α accentuates the variations of volumetric flux across A. The following is a brief outline of the key equations of the volumetric flux model for an inclined spray. The readers should refer to Ref. [15] for further details concerning this model.

The volumetric flux across spherical surface A' in Fig. 7 is given by

$$Q''_{sp}=\frac{Q}{2\pi H^2[1-\cos(\theta/2)]} \tag{1}$$

and across the test surface,

$$Q''=Q''_{sp}\frac{dA'}{dA} \tag{2}$$

In the present study, the area ratio dA'/dA is computed numerically for the locations of CHF commencements (end points of minor axis of impact ellipse) from the relevant geometrical parameters. Figure 8 shows the variation of dA'/dA with inclination angle α for each of the three nozzles tested in the present study. Notice the rapid decrease in area ratio with increasing inclination angle. Since Q''_{sp} in Eq. (2) is constant, Eq. (2) shows that Q'' decreases sharply with increasing inclination angle. For $\alpha=55$ deg (largest angle tested in the present study), Fig. 8 shows

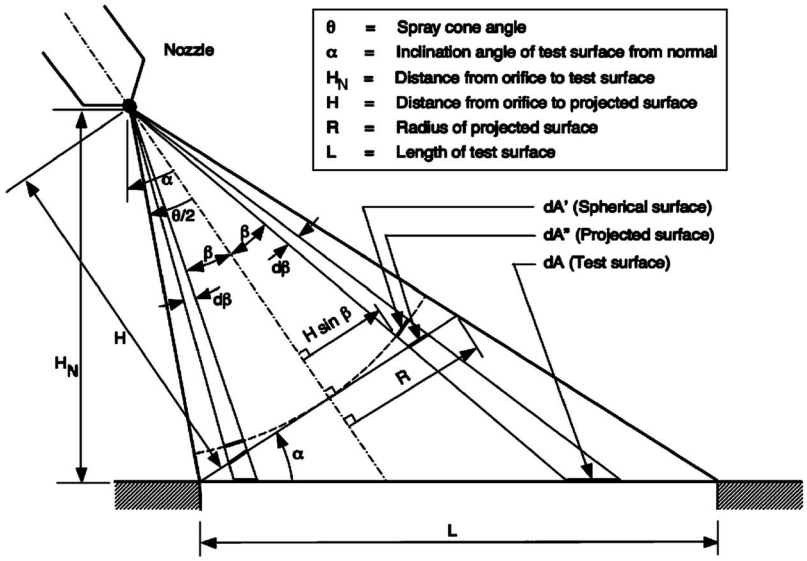

Fig. 7 Nomenclature for inclined spray model

that the spray flux along the impact surface is only about 20% of Q''_{sp}.

The relation between height H and length of the heater, L, is given by

$$\frac{H}{L} = \frac{1}{2}[\cos\alpha\cot(\theta/2) - \sin\alpha] \tag{3}$$

and because of the constraint of having the impact ellipse inscribe the test surface, the major axis of the ellipse, $2a$, is given by

$$2a = L \tag{4}$$

The minor axis $2b$ of the impact ellipse is given by

$$2b = L\cos\alpha\sqrt{1 - \tan^2\alpha\tan^2(\theta/2)} \tag{5}$$

Equation (5) shows that the minor axis of the impact ellipse decreases with increasing inclination angle. Knowing both the minor and the major axis, the following equation is derived for the area of the impact ellipse:

$$A_{ellipse} = \frac{\pi}{4}L^2\cos\alpha\sqrt{1 - \tan^2\alpha\tan^2(\theta/2)} \tag{6}$$

Figure 9 shows the variation of impact area with inclination angle for each of the nozzles tested. The substantial decrease of $A_{ellipse}$ with α appears to correlate well with the variation of CHF with α discussed earlier in relation to Figs. 6(*a*) and 6(*b*). However, this is only one aspect of the impact of α on CHF, given both the strong variations of volumetric flux across the test surface and the localized commencement of CHF along the end points of the minor axis of the impact ellipse. These complex effects will be reconciled in the next section in the development of a comprehensive model for spray CHF.

CHF Model

Using data for water, FC-72, and FC-87, Estes and Mudawar [7] developed a correlation for predicting local (point-based) CHF, $q''_{m,p}$, corresponding to locations of the impact area of a normal spray corresponding to the weakest volumetric flux:

$$\frac{q''_{m,p}}{\rho_g h_{fg} Q''} = 2.3\left(\frac{\rho_f}{\rho_g}\right)^{0.3}\left(\frac{\rho_f Q''^2 d_{32}}{\sigma}\right)^{-0.35}\left(1 + 0.0019\frac{\rho_f c_{p,f}\Delta T_{sub}}{\rho_g h_{fg}}\right) \tag{7}$$

where Q'' is the local volumetric flux along the outer perimeter of the impact circle of a normal spray. This correlation was also

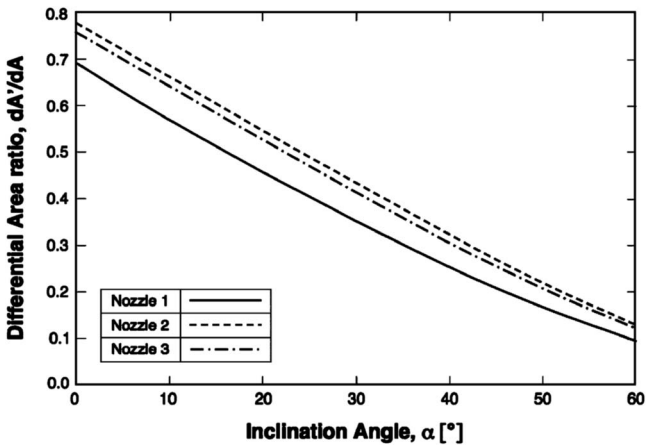

Fig. 8 Variation of differential area ratio corresponding to end points of the minor axis of impact ellipse with inclination angle for three nozzles

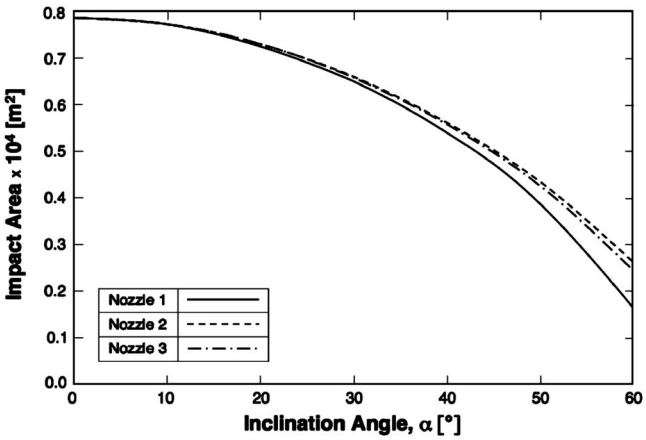

Fig. 9 Variation of spray impact area with inclination angle for three nozzles

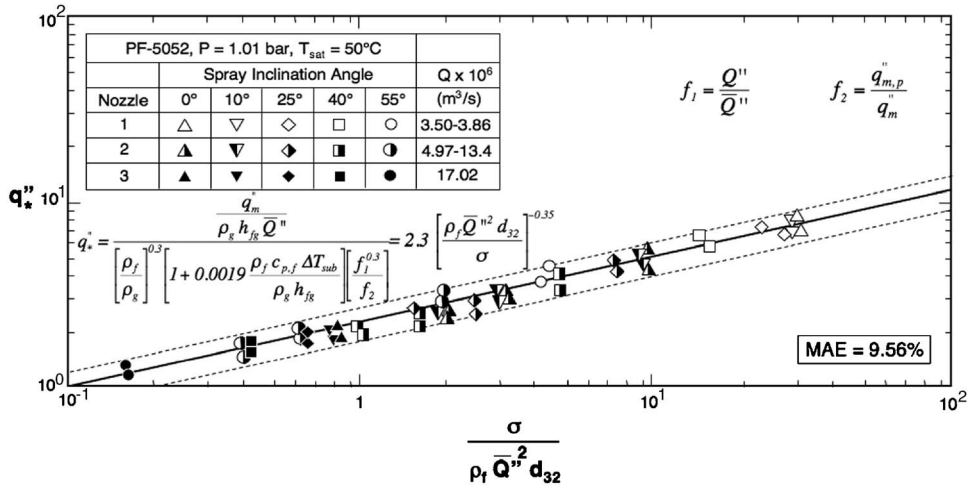

Fig. 10 Correlation of CHF data for PF-5052 for different orientations and nozzles based on average volumetric flux

validated by Rybicki and Mudawar [16] for upward facing PF-5052 sprays.

Recently, Visaria and Mudawar [15] validated this point-based CHF correlation for inclined sprays by identifying the locations of the impact ellipse corresponding to the weakest volumetric flux. On a geometrical basis alone, this point corresponds to the most downstream point of the major axis of the impact ellipse. However, dryout at this location as well as the entire downstream perimeter of the impact ellipse is delayed by the aforementioned lateral liquid flow. On the other hand, the two end points of the minor axis are the farthest points from the orifice that do not take advantage of the lateral liquid flow; CHF is therefore postulated to commence at these two end points. This means that Q'' in Eq. (7) should be determined at these two locations.

Of greater importance to electronics cooling is CHF based on total test surface area, i.e., device power divided by L^2. Unlike the point-based correlation approach presented by Visaria and Mudawar [15], a new approach is developed in the present study for calculating CHF values based on L^2 and volumetric flux averaged over the spray impact area. To accomplish this goal, Eq. (7) is rewritten as

$$\frac{q''_m}{\rho_g h_{fg} \bar{Q}''} = 2.3\left(\frac{\rho_f}{\rho_g}\right)^{0.3}\left(\frac{\rho_f \bar{Q}''^2 d_{32}}{\sigma}\right)^{-0.35}\left(1+0.0019\frac{\rho_f c_{p,f}\Delta T_{\text{sub}}}{\rho_g h_{fg}}\right) \times\left(\frac{f_1^{0.30}}{f_2}\right) \tag{8}$$

where

$$f_1 = \frac{Q''}{\bar{Q}''} \tag{9}$$

and

$$f_2 = \frac{q''_{m,p}}{q''_m} = \frac{1}{\left[\frac{\pi}{4}\cos\alpha\sqrt{1-\tan^2\alpha\tan^2(\theta/2)}\right]} \tag{10}$$

Q'' in Eq. (9) was calculated numerically using Eqs. (1) and (2), with the differential area ratio dA'/dA corresponding to the end points of the minor axis of the impact ellipse. Figure 10 shows excellent agreement between the CHF model predictions and experimental data for the three nozzles for different subcoolings, flow rates, and inclination angles. Virtually all the data fall within ±25% of the predictions with a mean absolute error of 9.56%.

Conclusions

This study provided a systematic method in predicting the effects of spray inclination on CHF from a 1.0×1.0 cm^2 test surface using PF-5052 as working fluid. This method includes an extension of a previous point-source spray model that was modified to incorporate the effects of nozzle inclination on volumetric flux distribution. Aided by extensive flow visualization studies, a method is devised to determine the location of CHF commencement on the test surface. This criterion is combined with a previous point-based CHF correlation to predict CHF for inclined sprays. Key findings from the study are as follows:

(1) An inclined spray produces an elliptical impact area. To achieve the highest possible CHF, the spray should be configured such that the impact ellipse just inscribes the test surface. Volumetric flux due to direct droplet impact greatly decreases with increasing contact angle, especially for the most downstream edge of the impact ellipse. However, this same region benefits from lateral liquid flow that is caused by the spray inclination. Two points that are both farthest from the nozzle orifice and do not benefit from the lateral liquid flow are the end points of the minor axis of the impact ellipse. CHF therefore commences at these two locations.
(2) CHF decreases monotonically with increasing spray inclination angle away from normal. This decrease is consistent with the trend of decreasing impact area and volumetric flux predicted by the volumetric flux model.
(3) Combining the results of the volumetric distribution model and flow visualization experiments with a previous point-based CHF correlation by Estes and Mudawar [7] and Visaria and Mudawar [15] provides a systematic and accurate means for predicting the effects of inclination angle on CHF.

Nomenclature

A = area of test surface
a = half-length of major axis of elliptical impact area
A' = area of spherical surface
A'' = area of projected surface
A_{ellipse} = area of impact ellipse
b = half-length of minor axis of elliptical impact area
c_p = specific heat

d_o = diameter of nozzle orifice
d_{32} = Sauter mean diameter (SMD)
f_1 = ratio of local to average volumetric flux
f_2 = ratio of point-based CHF to critical CHF based on total area (L^2) of test surface
H = radius of spherical surface
H_N = distance from orifice to test surface
h_{fg} = latent heat of vaporization
L = length (and width) of square test surface
Q = total volumetric flow rate of spray
Q'' = local volumetric flux across test surface
$\bar{Q}''$ = average volumetric flux across A_{ellipse}
q''_m = CHF based on total area (L^2) of test surface
$q''_{m,p}$ = point-based CHF
Q''_{sp} = local volumetric flux across spherical surface
R = radius of projected surface
T_f = liquid temperature at nozzle inlet
T_{sat} = saturation temperature based on test chamber pressure
ΔT_{sub} = difference between saturation temperature and inlet temperature, $T_{\text{sat}} - T_f$

Greek Symbols

α = inclination angle between spray axis and normal to test surface
β = angle used in uniform point-source model
θ = spray cone angle
ρ = density
σ = surface tension

Subscripts

f = liquid
g = vapor
m = maximum (CHF)
p = point based
sat = saturation
sub = subcooled

References

[1] Toda, S., 1972, "A Study in Mist Cooling," Trans. Jpn. Soc. Mech. Eng., **38**, pp. 581–588.
[2] Mudawar, I., and Valentine, W. S., 1989, "Determination of the Local Quench Curve for Spray Cooled Metallic Surfaces," ASM J. Heat Treating, **7**, pp. 107–121.
[3] Totten, G. E., Bates, C. E., and Clinton, N. A., 1993, *Handbook of Quenchants and Quenching Technology*, ASM International, Materials Park, OH.
[4] Hall, D. D., and Mudawar, I., 1995, "Predicting the Impact of Quenching on Mechanical Properties of Complex-Shaped Aluminum Alloy Parts," ASME J. Heat Transfer, **117**, pp. 479–488.
[5] Hall, D. D., and Mudawar, I., 1995, "Experimental and Numerical Study of Quenching Complex-Shaped Metallic Alloys With Multiple, Overlapping Sprays," Int. J. Heat Mass Transfer, **38**, pp. 1201–1216.
[6] Bernardin, J. D., and Mudawar, I., 2002, "A Cavity Activation and Bubble Growth Model of the Leidenfrost Point," ASME J. Heat Transfer, **124**, pp. 864–874.
[7] Estes, K. A., and Mudawar, I., 1995, "Correlation of Sauter Mean Diameter and CHF for Spray Cooling of Small Surfaces," Int. J. Heat Mass Transfer, **38**, pp. 2985–2996.
[8] Mudawar, I., and Estes, K. A., 1996, "Optimizing and Predicting CHF in Spray Cooling of a Square Surface," ASME J. Heat Transfer, **118**, pp. 672–679.
[9] Mudawar, I., 2001, "Assessment of High-Heat-Flux Thermal Management Schemes," IEEE Trans. Compon. Packag. Technol., **24**, pp. 122–141.
[10] Rini, D. P., Chen, R.-H., and Chow, L. C., 2002, "Bubble Behavior and Nucleate Boiling Heat Transfer in Saturated FC-72 Spray Cooling," ASME J. Heat Transfer, **124**, pp. 63–72.
[11] Lin, L., and Ponnappan, R., 2003, "Heat Transfer Characteristics of Spray Cooling in a Closed Loop," Int. J. Heat Mass Transfer, **46**, pp. 3737–3746.
[12] Lefebvre, A. H., 1989, *Atomization and Sprays*, Hemisphere, New York, NY.
[13] Silk, E. A., Kim, J., and Kieger, K., 2006, "Spray Cooling of Enhanced Surfaces: Impact of Structured Surface Geometry and Spray Axis Inclination," Int. J. Heat Mass Transfer, **49**, pp. 4910–4920.
[14] Li, B. Q., Cader, T., Schwarzkopf, J., Okamoto, K., and Ramaprian, B., 2006, "Spray Angle Effect During Spray Cooling of Microelectronics: Experimental Measurements and Comparison With Inverse Calculations," Appl. Therm. Eng., **26**, pp. 1788–1795.
[15] Visaria, M., and Mudawar, I., 2007, "Theoretical and Experimental Study of the Effects of Spray Inclination on Two-Phase Spray Cooling and Critical Heat Flux," Int. J. Heat Mass Transfer, doi: 10.1016/j.ijheatmasstransfer.2007.08.010.
[16] Rybicki, J. R., and Mudawar, I., 2006, "Single-Phase and Two-Phase Cooling Characteristics of Upward-Facing and Downward-Facing Sprays," Int. J. Heat Mass Transfer, **49**, pp. 5–16.
[17] Bernardin, J. D., Stebbins, C. J., and Mudawar, I., 1997, "Mapping of Impact and Heat Transfer Regimes of Water Drops Impinging on a Polished Surface," Int. J. Heat Mass Transfer, **40**, pp. 247–268.